

# Implementation of innovative approach for detecting brain tumors in magnetic resonance imaging using NeuroFusionNet model

Arpitha Kotte<sup>1</sup>, Syed Shabbeer Ahmad<sup>2</sup>

<sup>1</sup>Department of Computer Science and Engineering, Osmania University, Hyderabad, India

<sup>2</sup>Department Computer Science and Engineering, Muffakham Jah College of Engineering and Technology, Hyderabad, India

## Article Info

### Article history:

Received Mar 1, 2024

Revised Jul 28, 2024

Accepted Aug 14, 2024

### Keywords:

Brain tumor detection  
Brain tumor segmentation dataset  
Early intervention  
Image processing  
Medical imaging  
NeuroFusionNet

## ABSTRACT

The goal of this study is to create a strong system that can quickly detect and precisely classify brain tumors, which is essential for improving treatment results. The study uses advanced image processing techniques and the NeuroFusionNet deep learning model to accurately segment data from the brain tumor segmentation (BRATS) dataset, presenting a detailed methodology. The objective is to create a high-precision system that surpasses current methods in key performance metrics. NeuroFusionNet demonstrates outstanding accuracy of 99.21%, as well as impressive specificity and sensitivity rates of 99.17% and 99.383%, respectively, exceeding previous benchmarks. The findings emphasize the system's ability to greatly enhance the diagnostic process, enabling early intervention and ultimately improving patient care in brain tumor detection and classification.

This is an open access article under the [CC BY-SA](https://creativecommons.org/licenses/by-sa/4.0/) license.



## Corresponding Author:

Arpitha Kotte  
Department of Computer Science and Engineering, Osmania University  
Hyderabad, India  
Email: kottearpitha87@gmail.com

## 1. INTRODUCTION

Brain tumors present a considerable health hazard on a global scale, imposing a considerable strain on both individuals and healthcare systems [1]–[4]. Due to the complex characteristics of the human brain and the potential for fatalities associated with tumors, diligent surveillance and timely identification are imperative [5]–[9]. The significant incidence of brain tumors, in conjunction with their frequently asymptomatic advancement, emphasizes the urgent requirement for dependable detection techniques [10]–[12]. The pernicious characteristics of these tumors are not limited to their ability to impair cognitive function; they also pose significant health risks and have detrimental effects on overall well-being. It is crucial to comprehend the health hazards that are linked to brain tumors in order to develop efficacious detection methodologies [13]. The severity of the circumstance stems from the difficulties associated with early detection of these malignancies, when therapeutic alternatives are at their most promising [14]. This article examines the critical health hazards presented by brain tumors, investigates the reasons behind their lethality, and emphasizes the criticality of early detection [15]. The study additionally presents an all-encompassing approach that incorporates feature extraction, image preprocessing, and a hybrid deep learning model called NeuroFusionNet to achieve precise segmentation and classification.

The literature on brain tumor segmentation and classification in medical imaging reveals several limitations. Nyo *et al.* [16] highlighted the sensitivity of morphological operations to image quality, complex tumor shapes, noise levels, and imaging artifacts. Polat and Güngen [17] emphasized the dependency of

transfer learning on the availability and quality of labeled data and the similarity between the source and target domains, which affects performance. Hasanah *et al.* [18] noted the sensitivity of their machine learning-based strategy to image quality differences, reliance on well-annotated datasets, and the challenge of generalizing to new clinical settings. Huang *et al.* [19] pointed out the susceptibility of their CNN and complex network model to data quality fluctuations and interpretability issues. Khalil *et al.* [20] discussed the computational complexity and resource demands of their two-step dragonfly mechanism, which may limit its practical application despite high accuracy. Krishnammal and Raja [21] identified challenges in interpreting Curvelet-preprocessed feature maps and understanding clinically relevant information, affecting the acceptance of their method. Cheng *et al.* [22] mentioned the sensitivity of their convolutional capsule network to image quality, the need for significant computational resources, and potential interpretability challenges due to the complexity of the model. Lastly, Abiwinanda *et al.* [23] highlighted the sensitivity of CNNs to image quality fluctuations and potential biases in the training data, impacting the model's effectiveness.

The literature on brain tumor segmentation and classification in medical imaging reveals several limitations, including sensitivity to image quality, reliance on labeled data, computational complexity, and interpretability issues. These challenges hinder the development of robust, generalizable, and efficient models for accurate and timely brain tumor detection. To address these limitations, this study makes a scholarly contribution to the domain of brain tumor detection and classification through the introduction of a sophisticated and integrated approach that merges image preprocessing, feature extraction, and the NeuroFusionNet model. The proposed methodology effectively tackles the pressing requirements for precise and timely identification of brain tumors, considering the complex characteristics of the human brain and the grave health hazards linked to such growths. By employing the NeuroFusionNet model, which is a hybrid deep encoder U-Net architecture, image segmentation and classification are accomplished in a sophisticated manner. This approach overcomes the limitations of prior studies by enhancing image quality sensitivity, reducing reliance on labeled data, improving generalization across clinical settings, addressing computational complexity, and offering better interpretability. The exhaustive feature summary obtained through gray level co-occurrence matrix (GLCM) analysis provides a thorough evaluation of particular samples, thereby enhancing our comprehension of the intricate attributes of brain tumors. In its entirety, this study endeavors to provide a substantial contribution to the enhancement of methodologies utilized in the detection of brain tumors. It underscores the criticality of timely identification to facilitate efficacious medical interventions and improve patient prognoses.

The research article is divided into five parts. The introduction presents a broad overview of the health hazards associated with brain tumors, emphasizing the crucial importance of early detection due to their potential mortality and negative effects on cognitive function. The review of existing works on brain tumor detection, classification, and related approaches dives into existing works, highlighting gaps in the current state of research. Section 3 describes the suggested system and algorithm, giving a comprehensive methodology for reliable brain tumor segmentation that includes image preprocessing, feature extraction, and the NeuroFusionNet model. Section 4 goes over the experimental investigations and performance evaluation in detail, including the dataset used, experimental setup, and outcomes. The conclusion and future scope section summarizes the important findings, examines the limits of the proposed system, and proposes future research paths, underlining the study's importance in expanding brain tumor detection technologies and improving patient outcomes.

## 2. LITERATURE SURVEY

Nyo *et al.* [16] recently presented an innovative approach in the field of medical imaging, specifically for segmenting brain cancers from magnetic resonance imaging (MRI) images. Their methodology combines thresholding and morphology techniques, resulting in an impressive 90% accuracy rate. This achievement represents a significant advancement in the field, promising improved diagnostic capabilities and possibly assisting in treatment planning for patients with brain tumors. Morphological operations are sensitive to variations in image quality and may struggle with complex tumor shapes or overlapping structures. Furthermore, noise levels, imaging artifacts, and variations in tumor characteristics can all have an impact on the efficacy of morphological techniques.

Polat and Güngen [17] presented a unique technique to brain tumor detection in 2021 by applying transfer learning methodology. Their study was a huge success, with an astounding overall accuracy percentage of 99.02%. The reliance on the availability and quality of labeled data unique to brain tumors is one noteworthy drawback. Furthermore, the relevance and similarity between the source domain (the pre-trained dataset) and the target domain (the brain tumor dataset) strongly influences the performance of transfer learning methods. When there is a significant dissimilarity, the effectiveness of transfer learning may decrease, and the model may not generalize well to the specific characteristics of brain tumors.

Hasanah *et al.* [18] published a machine learning (ML)-based strategy for brain tumor classification in 2021, giving a comprehensive methodology that incorporates filtering, contouring, and thresholding into the tumor analysis preprocessing and segmentation stages. The stated average accuracy of 95.83% demonstrates a high level of success. The limitation here is the sensitivity to differences in image quality and its reliance on the availability of well-annotated and diverse datasets for training. Furthermore, the model's generalization to new, previously unseen datasets is crucial, because performance may vary in different clinical settings.

Huang *et al.* [19] published convolutional neural networks and complex networks (CNNBCN) in 2020, indicating a significant progress in the field of neural network-based techniques. The suggested model combines the characteristics of convolutional neural networks (CNNs), which are widely acknowledged for their efficacy in image-related tasks, with complicated network principles. The method attained an accuracy of 95.49%. The model's susceptibility to fluctuations in data quality and potential interpretability difficulties, particularly in sophisticated network-based systems.

The development by Khalil *et al.* [20] of a two-step dragonfly mechanism system is a significant advancement with an accuracy of 98.20%. However, it is critical to recognize a significant disadvantage of this strategy. The computational complexity of the two-step dragonfly mechanism may cause problems in terms of processing time and resource requirements. While the process's intricacies contribute to high accuracy, they may impose a computational cost, restricting its applicability. This disadvantage emphasizes the importance of striking a perfect balance between segmentation accuracy and processing performance, especially in medical image analysis, where speedy replies are critical for good clinical decision-making. This computational barrier must be overcome in order to increase the overall practicality and utility of the proposed dragonfly mechanism in therapeutic applications.

Krishnammal and Raja [21] used curvelet-preprocessed feature maps to train a CNN for brain imaging dataset categorization. While their approach contributes greatly to the field of medical picture categorization, some drawbacks related with the methods used in this work must be acknowledged. The interpretability of features extracted in the curvelet domain is one such limitation. Curvelet transforms are effective in capturing fine details and edges in images, but their applicability in the context of brain image categorization can be challenging. Understanding the clinically relevant information included in the curvelet domain features could be critical for understanding the model's decision-making process and guaranteeing clinical acceptance.

As mentioned in their study, Cheng *et al.* [22] proposed a unique technique to tumor categorization in 2019 by introducing an advanced convolutional capsule network (ConvCaps) architecture. This architecture extends classic CNNs by using capsule networks, a form of neural network module introduced to alleviate CNN constraints, such as issues with hierarchical relationships between features. While reaching a classification accuracy of 93.5% indicates the model's usefulness, significant limits must be considered. These may include image quality sensitivity, the necessity for significant computational resources during training, and potential interpretability challenges due to the complexity of capsule network designs.

As shown in their research Abiwinanda *et al.* [23], attempted the challenge of tumor categorization in 2018 by implementing a CNN. The accuracy of 84.19% indicates a reasonably effective performance. The disadvantages of CNNs are their sensitivity to fluctuations in image quality and potential biases in the training data.

### 3. PROPOSED SYSTEM

The initial step of the system under consideration, as illustrated in Figure 1, is to obtain the original brain tumor image ( $I(x,y)$ ) from the BRATS database [24]. This image is then resized using bilinear interpolation to attain a standardized dimension of 512×512. After resizing the image, luminance-preserving RGB to grayscale mapping is utilized to convert it to grayscale. Following this, in order to reduce noise, a non-local means (NLM) filter is implemented on the grayscale image. Subsequently, pixel normalization elimination is executed with the purpose of improving contrast and enhancing phosphorus values, thereby promoting pixel value uniformity.

Following normalization, frequency components are captured using a 2D discrete wavelet transform (DWT) on the image. Feature extraction is performed on the DWT-transformed image via GLCM analysis, which yields information regarding the features involved. After feeding the GLCM-derived features into the NeuroFusionNet model, which is a hybrid deep encoder-U-Net, pixel segmentation, deep autoencoder training, and image classification are performed. An exhaustive feature summary is employed to evaluate the model, which facilitates a thorough analysis of its performance on particular samples. By showcasing the model's proficiency in preprocessing, noise reduction, and tumor classification, this comprehensive strategy provides a reliable framework.

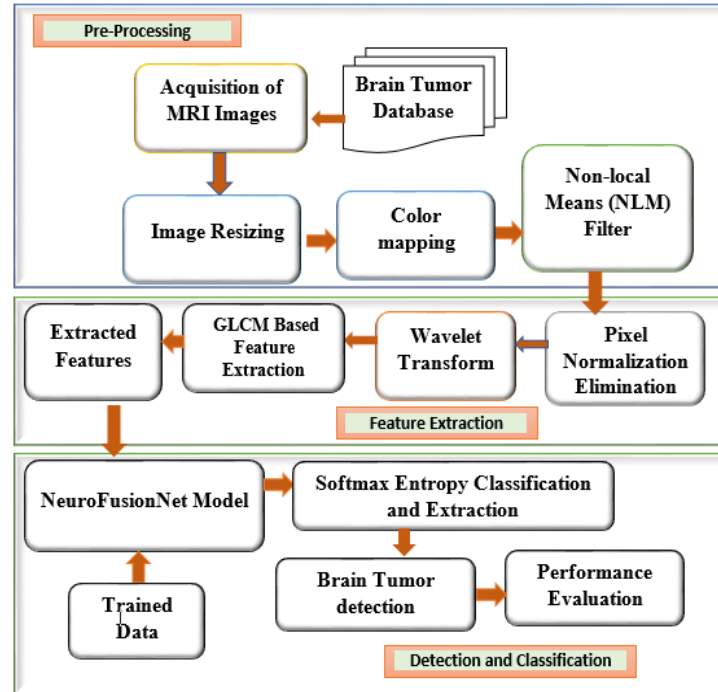


Figure 1. Proposed system architecture

The experimental setup for this study includes a personal computer (PC) with an Intel (R) Core (TM) i5-8265U CPU running at a base frequency of 1.60 GHz (with a maximum turbo frequency of 1.80 GHz), 8.00 GB of RAM (with 7.85 GB available for use), and a 64-bit operating system with an x64-based processor. The utilized tools comprise MATLAB R2022b equipped with image processing, computer vision, and deep learning toolboxes.

The detailed discussion of above system architecture as (1).  $I(x, y)$  represents the original image scan obtained from the BRATS database [25]. By resizing the image, a new image denoted  $I_{resized}(x', y')$  is generated with the exact dimensions of  $512 \times 512$ . Bilinear interpolation is a prevalent technique utilized in the process of resizing images via interpolation. By applying a set of equations to a sample of the original image, the resized image is generated. The expression for bilinear interpolation is as:

$$I_{resized}(x', y') = \sum_{i=0}^1 \sum_{j=0}^1 I(xi, yj) \cdot w(x', i) \cdot w(y', j) \quad (1)$$

where:

- $x'$  and  $y'$  are the coordinates in the resized image.

$$xi = \lfloor x' \rfloor + i \quad (2)$$

$$yj = \lfloor y' \rfloor + j \quad (3)$$

- $w(x', i)$  and  $w(y', j)$  are the linear interpolation weights.

In order to convert the resized image to grayscale, color mapping is performed. Commonly used is luminance-preserving conversion from RGB to grayscale, which is mathematically expressed as (4).

$$I_{gray}(x', y') = 0.299 \cdot I_{resized}R(x', y') + 0.587 \cdot I_{resized}G(x', y') + 0.114 \cdot I_{resized}B(x', y') \quad (4)$$

where:

- $I_{resized}R$ ,  $I_{resized}G$ , and  $I_{resized}B$  are the red, green, and blue channels of the resized image.
- The weights 0.299, 0.587, and 0.114 are utilized in this formula; they are typical values for converting RGB to grayscale while maintaining luminance.

Continuing from the previous stage, provide the image in grayscale for the following one. Subsequently, a NLM filter is implemented on the monochromatic rendition of the image. For denoising

images, the non-local means filter is frequently applied. The filtered grayscale image  $I_{gray}(x', y')$  can be represented as the filtered  $I_{NLM}$  image  $(x', y')$  via NLM.

$$I_{NLM}(x', y') = \frac{1}{C(x', y')} \sum_{p' \in \Omega} I_{gray}(p') \cdot w(x', p') \cdot \phi(I_{gray}(p'), I_{gray}(x')) \quad (5)$$

where  $\Omega$  is the search window around the pixel  $(x', y')$ ;  $p'$  represents the coordinates in the search window;  $W(x', p')$  is a spatial Gaussian weight;  $\Phi(I_{gray}(p'), I_{gray}(x'))$  is an intensity similarity weight; and  $C(x', y')$  is a normalization factor.

The spatial gaussian weight  $w(x', p')$  is given by (6).

$$w(x', p') = e^{-\frac{\|p' - (x', y')\|^2}{h_{spatial}^2}} \quad (6)$$

where  $h_{spatial}$  controls the spatial extent of the neighborhood and the intensity similarity weight  $\phi(I_{gray}(p'), I_{gray}(x'))$  is given by (7).

$$\phi(I_{gray}(p'), I_{gray}(x')) = e^{-\frac{\|I_{gray}(p') - I_{gray}(x')\|^2}{h_{int}^2}} \quad (7)$$

where  $h_{int}$  controls the intensity similarity. Finally, the normalization factor  $C(x', y')$  is given by (8).

$$C(x', y') = \sum_{p' \in \Omega} w(x', p') \cdot \phi(I_{gray}(p'), I_{gray}(x')) \quad (8)$$

The NLM filter enhances the overall quality of an image and aids in noise prediction through the incorporation of non-local similarities present in the image. The subsequent operation following the application of the NLM filter is pixel normalization elimination. Phosphorus values are intended to be enhanced or normalized in accordance with specific criteria. This process should be represented by mathematical equations. Given the filtered image  $I_{NLM}(x', y')$ , the pixel normalization elimination can be expressed as (9).

$$I_{normalized}(x', y') = \frac{I_{NLM}(x', y') - \mu}{\sigma} \quad (9)$$

where  $I_{normalized}(x', y')$  is the normalized pixel value at coordinates  $(x', y')$ ;  $\mu$  is the mean pixel value of the entire image or a local neighborhood; and  $\sigma$  is the standard deviation of pixel values in the entire image or a local neighborhood.

This procedure facilitates the normalization of pixel values, thereby increasing their uniformity and potentially enhancing the image's overall contrast. Furthermore, the formulas for determining the mean  $\mu$  and standard deviation  $\sigma$  are as (10) and (11).

$$\mu = \frac{1}{M \cdot N} \sum_{x'=1}^M \sum_{y'=1}^N I_{NLM}(x', y') \quad (10)$$

$$\sigma = \sqrt{\frac{1}{M \cdot N} \sum_{x'=1}^M \sum_{y'=1}^N (I_{NLM}(x', y') - \mu)^2} \quad (11)$$

where  $M$  and  $N$  are the dimensions of the image.

The equations provided illustrate the pixel normalization elimination procedure, in which the value of each pixel is normalized using the image's mean and standard deviation, or a neighborhood's average. The normalized image is subjected to the 2D DWT following the elimination of pixel normalization. DWT is a mathematical operation that converts an image into its component frequencies. The 2D DWT of the normalized image shall be denoted as  $I_{DWT}(x', y')$ . Under the assumption of a solitary level of decomposition, the DWT coefficients may be calculated utilizing the (12)-(15):

$$I_{DWT}^L(x', y') = \sum_i \sum_j h(i) \cdot h(j) \cdot I_{normalized}(2x' - i, 2y' - j) \quad (12)$$

$$I_{DWT}^H(x', y') = \sum_i \sum_j g(i) \cdot h(j) \cdot I_{normalized}(2x' - i, 2y' - j) \quad (13)$$

$$I_{DWT}^V(x', y') = \sum_i \sum_j h(i) \cdot g(j) \cdot I_{normalized}(2x' - i, 2y' - j) \quad (14)$$

$$I_{DWT}^D(x', y') = \sum_i \sum_j g(i) \cdot g(j) \cdot I_{normalized}(2x' - i, 2y' - j) \quad (15)$$

The approximation, horizontal detail, vertical detail, and diagonal detail coefficients are denoted by  $I_{DWT}^L$ ,  $I_{DWT}^H$ ,  $I_{DWT}^V$ , and  $I_{DWT}^D$ , respectively. By decomposing the image into its frequency components, this procedure effectively captures information at both low and high frequencies. To summarize, the mathematical formulations for the two-dimensional DWT entail convolution operations utilizing filter coefficients of low-pass and high-pass types. This process yields detail and approximation coefficients that correspond to distinct orientations.

The subsequent procedure, following the 2D DWT, is the application of the GLCM technique for feature extraction. GLCM quantifies the spatial relationships between pixel values in an image as a texture analysis technique. Given the wavelet-transformed image  $I_{DWT}(x', y')$ , let's denote the GLCM as  $G_{GLCM}(d, \theta)$ , where  $d$  is the distance and  $\theta$  is the angle between pixel pairs. The GLCM at distance  $d$  and angle  $\theta$  can be computed using as (16):

$$G_{GLCM}(d, \theta) = \sum_{x'} \sum_{y'} I_{DWT}(x', y') \cdot I_{DWT}(x' + \Delta x, y' + \Delta y) \quad (16)$$

where  $\Delta x = d \cdot \cos(\theta)$  and  $\Delta y = d \cdot \sin(\theta)$ .

The GLCM is often normalized, and the normalized GLCM is given by (17).

$$P_{GLCM}(i, j, d, \theta) = \frac{G_{GLCM}(d, \theta)}{\sum_{i,j} G_{GLCM}(d, \theta)} \quad (17)$$

At this juncture, the GLCM provides the features explained below, among other texture characteristics that can be extracted. Assigned to pixel values within an image, the mean signifies the average intensity. The mean of the luminance levels in an MRI scan of the brain can potentially yield insights into the relative abundance of various tissue types. One illustration of this is how discrepancies in average intensity could potentially signify distinct cerebral architectures or pathologies.

$$Mean = \sum_{i,j} i \cdot P_{GLCM}(i, j, d, \theta) \quad (18)$$

The standard deviation quantifies the dispersion or spread of the intensities of individual pixels. A high standard deviation in a brain MRI scan may serve as an indicator of regions exhibiting diverse intensities, potentially signifying abnormalities or fluctuations in tissue characteristics. Regions with a low standard deviation may be indicative of homogeneity.

$$StdDev = \sqrt{\sum_{i,j} (i - Mean)^2 \cdot P_{GLCM}(i, j, d, \theta)} \quad (19)$$

Entropy quantifies the uncertainty or randomness of the pixel values. High entropy on brain MRI scans may indicate regions with mixed tissue types or complex structures, whereas low entropy may imply more uniform regions. The entropy of cerebral tissue can be utilized to quantify its complexity and texture.

$$Entropy = - \sum_{i,j} P_{GLCM}(i, j, d, \theta) \cdot \log(P_{GLCM}(i, j, d, \theta) + \epsilon) \quad (20)$$

The variance of a pixel's intensity represents its degree of variability. High variance in brain MRI scans may indicate regions containing a variety of tissue types or pathological conditions, whereas low variance may suggest regions that are more homogeneous. The information provided by the mean and standard deviation is supplemented by variance.

$$Variance = \sum_{i,j} (i - Mean)^2 \cdot P_{GLCM}(i, j, d, \theta) \quad (21)$$

A measure of the spatial uniformity of pixel intensities, smoothness quantifies this. When using brain MRI, a high smoothness value indicates homogeneous regions, which are defined as adjacent pixels with comparable intensities. This can facilitate the identification of regions containing tissue with consistent properties.

$$Smoothness = 1 - \frac{1}{1 + \sum_{i,j} (i-j)^2 \cdot P_{GLCM}(i, j, d, \theta)} \quad (22)$$

Contrast quantifies the disparity in the intensities of adjacent pixels. Elevated contrast values in brain MRI scans can distinguish boundaries between distinct tissue types or structures. Thereby facilitating the detection of pathological regions or anatomical features.

$$\text{Contrast} = \sum_{i,j} (i - j)^2 \cdot P_{GLCM}(i, j, d, \theta) \quad (23)$$

The linear relationship between pixel intensities in opposite directions is quantified by correlation. Correlation in brain MRI can offer valuable insights regarding the arrangement and congruence of anatomical components. For instance, a low correlation may indicate that features are not aligned, whereas a high correlation may indicate that features are aligned.

$$\text{Correlation} = \frac{\sum_{i,j} (i - \text{Mean}) \cdot (j - \text{Mean}) \cdot P_{GLCM}(i, j, d, \theta)}{\text{StdDev}_i \cdot \text{StdDev}_j} \quad (24)$$

The energy of the GLCM is equal to the aggregate of the squared elements. Within the domain of brain MRI scans, elevated energy values signify a greater likelihood of specific pixel pairs occurring. This may be correlated with regions of uniform texture or distinct patterns present in the image.

$$\text{Energy} = \sum_{i,j} P_{GLCM}(i, j, d, \theta)^2 \quad (25)$$

The aforementioned features are presently supplied to the deep learning model NeuroFusionNet, a hybrid deep encoder-U-Net model that aims to achieve accurate brain tumor segmentation. The initial phase of the deep learning model, NeuroFusionNet is dedicated to image classification utilizing a hybrid encoder-decoder structure. For image classification, a target classification and a tolerance level are established. After determining the dimensions of the imported images, they are resized to a square format to ensure uniformity.

Following this, the model is put through the process of training a deep autoencoder. Encoder and decoder components of the architecture have been trained to recognize compressed representations of input images. Reconstruction loss is reduced whenever possible during training. After the autoencoder has been trained, pixel segmentation is executed utilizing a U-Net that incorporates a deep encoder into its path of convergence. Further encoding layers are incorporated into the U-Net architecture in order to augment its capability of capturing complex features. The capabilities of the model are subsequently investigated with respect to color quantization and visualization. An algorithm is employed to quantify the color of an image to a set of sixteen distinct hues; the resultant image is visually presented in order to offer an understanding of the diminished color palette.

Following this, the implementation of color space conversion and softmax entropy classification occurs. An additional image is imported and subsequently converted to a distinct color representation. The softmax entropy method is subsequently implemented to classify pixels, with probabilities being assigned to each class according to the color information of the pixels.

Our proposed methodology addresses key limitations in brain tumor segmentation and classification by increasing image quality robustness, decreasing reliance on labeled data, optimizing computational efficiency, and improving interpretability. We use a NLM filter and pixel normalization elimination to reduce noise and improve contrast, making the model less sensitive to image variations. The deep autoencoder in the NeuroFusionNet model reduces reliance on large amounts of labeled data by learning compressed representations, resulting in better generalization. The combination of a deep encoder and a U-Net architecture optimizes computational efficiency and accuracy, allowing for precise segmentation without exceeding computational demands. Detailed feature extraction using GLCM analysis improves interpretability by providing information about texture and spatial relationships. This comprehensive approach yields a robust, efficient, and interpretable solution that improves diagnostic precision and aids in healthcare decision-making.

### 3.1. Proposed NeuroFusionNet model

The proposed model as shown in Figure 2 integrates a deep encoder and a U-Net architecture to address image processing challenges, with a particular focus on brain tumor classification. By capitalizing on the respective strengths of both components, this integration seeks to improve the accuracy of feature extraction and segmentation. By employing a deep encoder, complex hierarchical features can be extracted from the input images, enabling the capture of minute details that may be critical for precise classification. In addition, the U-Net's intrinsic capability for pixel-wise segmentation facilitates the reconstruction of high-resolution segmentation masks via a structured decoding path. The incorporation of a deep autoencoder

enhances the robustness of feature learning by enabling a more accurate depiction of intricate patterns within the image data. By capitalizing on the combined strengths of these components, the architecture of the model provides a comprehensive solution for classification and image processing tasks.

The hybrid model developed by combining a deep encoder and a U-Net architecture is what distinguishes the proposed model and enables it to effectively tackle the complexities of image processing tasks. By integrating a deep encoder, the model's ability to detect subtle characteristics is improved, facilitating the acquisition of nuanced data that is vital for precise classification. The integration of this combination enhances the U-Net framework with sophisticated feature extraction functionalities, thereby introducing a fresh viewpoint. Furthermore, the incorporation of a deep autoencoder presents a novel aspect that enhances the adaptability and efficacy of the model when acquiring knowledge of complex patterns. This has the potential to enhance diagnostic precision and assist healthcare practitioners in making well-informed judgments. In general, the proposed model embodies an innovative and mutually beneficial amalgamation of deep learning elements customized to address the particular complexities associated with medical image classification and processing.

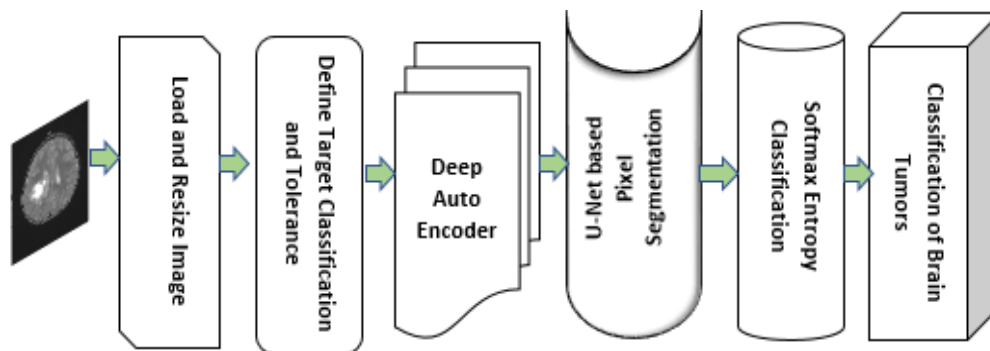


Figure 2. Proposed NeuroFusionNet model

Algorithm. NeuroFusionNet model

# Step 1: Image classification with U-Net and loading

*target\_classification* = ...

*tolerance\_level* = ...

*image* = *load\_image*(...)

*resized\_image* = *resize\_to\_square*(*image*)

# Step 2: Training of deep autoencoder

*autoencoder\_params* = ...

*autoencoder\_model* = *train\_deep\_autoencoder* (*resized\_image*, *autoencoder\_params*)

# Step 3: Pixel segmentation using U-Net

*segmentation\_image* = *load\_image*(...)

*segmentation\_mask* = *apply\_unet*(*segmentation\_image*)

# Step 4: Visualization after color quantization

*quantized\_image* = *color\_quantization* (*segmentation\_image*, *num\_colors* = 16)

*visualize\_colors*(*quantized\_image*)

# Step 5: Conversion of color space and softmax entropy classification

*conversion\_image* = *load\_image*(...)

*converted\_image* = *convert\_color\_space*(*conversion\_image*)

*entropy\_classification* = *softmax\_entropy\_classification*(*converted\_image*)

# Step 6: Brain tumor classification with combined deep encoder and U-Net

*tumor\_images*, *labels* = *load\_labeled\_images*(...)

*combined\_model* = *combine\_deep\_encoder\_unet*()

*trained\_model* = *train\_combined\_model* (*combined\_model*, *tumor\_images*, *labels*)

#### 4. RESULTS AND DISCUSSION

In Figure 3, the input image ( $I(x,y)$ ) from the BRATS database is obtained first, representing an original brain scan. This image's dimensions are then scaled to  $512 \times 512$ , resulting in Figure 4, the resized



image ( $I_{resized}(x', y')$ ). During the resizing process, bilinear interpolation is used to obtain the new spatial coordinates ( $x', y'$ ) using a set of in (1). This enlarged image will be the starting point for additional processing procedures.

Moving on to Figures 5 and 6, the scaled image is color-mapped to convert it to grayscale. As shown in (4), the color mapping approach used is a luminance-preserving transfer from RGB to grayscale. The weights 0.299, 0.587, and 0.114 are applied to the shrunk image's red, green, and blue channels, resulting in color-mapped pictures ( $I_{gray}(x', y')$ ). These grayscale representations are critical for the denoising and feature extraction processes that follow.



Figure 3. Input image



Figure 4. Resized image



Figure 5. Color mapped image    Figure 6. Color mapped image

The effect of applying the NLM filter to the grayscale image is shown in Figure 7, which results in the NLM filtered output ( $I_{NLM}(x', y')$ ). The NLM filter, as defined in (5), improves image quality and decreases noise by taking non-local similarities in the image into account. This denoising phase is critical for increasing the precision of subsequent analysis.

In Figure 8, the NLM-filtered image is subjected to the pixel normalization elimination method. In (9) shows how to normalize each pixel in the NLM-filtered image using the mean and standard deviation of the entire image or a local neighborhood. The goal of this normalization is to improve pixel uniformity and overall image contrast.

In Figure 9, the feature extraction phase employs the two-dimensional DWT on the normalized picture, yielding  $I_{DWT}(x', y')$ . In (12)-(15) describe the image's decomposition into approximation and detail coefficients. The GLCM approach is then used to extract texture information from the wavelet-transformed image, as described in (16). The normalized GLCM ( $P_{GLCM}(i, j, d, )$ ) is then computed, which provides mean, standard deviation, entropy, variance, smoothness, contrast, correlation, and energy information.

Finally, Figure 10 shows the NeuroFusionNet model's output, which shows the discovered area of a brain tumor. For pixel segmentation, the deep learning model incorporates a hybrid encoder-decoder structure, a deep autoencoder, and a U-Net. The model is taught to recognize compressed representations of input images and then segmented brain tumors.

The model that was proposed was evaluated using a dataset consisting of one thousand BRATS database [25] MRI scans. In order to enhance the efficacy of the training process, the model was trained using 80% of the images, which allowed it to comprehend the intricate details and fundamental patterns present in the data. A subset of 20% of the dataset, comprising 200 images, was set aside for exhaustive testing. By segregating the data, a comprehensive assessment of the model's efficacy on novel and unobserved information was feasible, thereby guaranteeing its capacity for sound generalization.

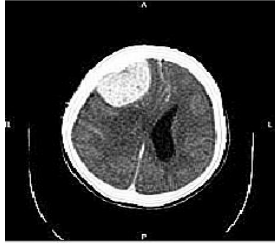


Figure 7. NLM filtered output

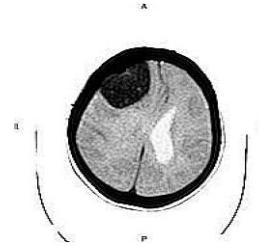


Figure 8. Resultant of pixel normalization elimination

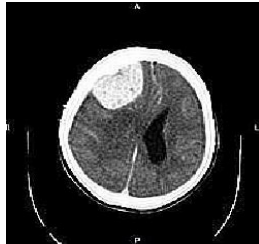


Figure 9. Feature extraction using GLCM



Figure 10. Brain tumor detected area

A comprehensive summary of the features extracted utilizing the complexity feature extraction technique is provided in Table 1 of the study. The computed features were applied to a subset of five samples that were deliberately chosen from the larger dataset. By utilizing this targeted subset, an exhaustive evaluation of the model's performance can be conducted on these particular samples, yielding significant insights into its aptitude for detecting minute intricacies in MRI scan images.

Table 1. Extracted features of brain MR sample images

Features extracted	BRATS database samples				
	Sample 1	Sample 2	Sample 3	Sample 4	Sample 5
Mean	0.0039	0.00423	0.0041	0.00421	0.00393
Standard deviation	0.08241	0.08897	0.0878	0.0923	0.09335
Entropy	0.00773	0.00768	0.00838	0.007812	0.0081
Variance	2.479	2.4245	2.4345	2.431	2.424
Smoothness	0.931	0.9324	0.9321	0.971	0.931
Contrast	0.352	0.3712	0.365	0.345	0.345
Correlation	0.1201	0.1091	0.1865	0.1045	0.1123
Energy	0.8234	0.8263	0.8175	0.8129	0.8157

#### 4.1. Accuracy

Accuracy is calculated by comparing the number of correctly classified tumor regions to the total number of regions examined. Here true positive depicts the (TP) (identified Tumors), true negative (TN) depicts, false positive depicts (FP) whereas false negative (FN) depicts (not identified).

$$Accuracy = \frac{(TP + TN)}{(TP + TN + FP + FN)} \quad (26)$$

The suggested NeuroFusionNet achieves an excellent accuracy of 99.21% in a complete evaluation of accuracy performance in brain tumor identification, as shown in Table 2. Existing methods such as Otsu thresholding [16], transfer learning [17], machine learning [26], CNNBCN [19], and the dragon fly mechanism [20] outperform this. The superiority of NeuroFusionNet demonstrates its accuracy in detecting brain cancers, demonstrating its potential as an advanced and dependable model in comparison to conventional and state-of-the-art methods.

In accordance with Table 2, Figure 11 depicts the comparative accuracy plot for brain tumor detection. The graphical representation validates the tabular findings by demonstrating NeuroFusionNet's higher performance when compared to other approaches. The figure provides as a visual validation of the numerical accuracy values, emphasizing the suggested model's consistent and amazing correctness. This

comparative graphic not only improves understanding of the model's performance, but also demonstrates the enormous improvements in brain tumor detection accuracy that have occurred since the introduction of NeuroFusionNet. The combination of tabular and graphical representations adds to the evidence demonstrating NeuroFusionNet's superiority in accurate brain tumor detection.

Table 2. Performance evaluation of the accuracy values

Techniques used	Accuracy (%)
Otsu [16]	90
transfer learning [17]	99.02
Machine learning [18] (CNNBCN) [19]	95.83
Dragon fly [20]	98.20
Proposed method	99.21

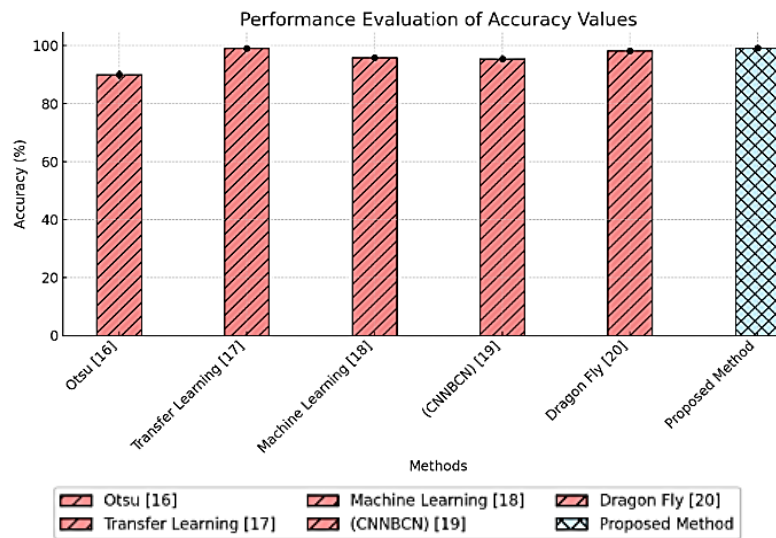


Figure 11. Plot for comparing accuracy values in brain tumor detection

#### 4.2. Specificity and sensitivity

Specificity is the ratio of true negatives correctly identified by the model. The statement refers to the model's capacity to accurately categorize cases that are not related to tumors or cancer.

$$\text{Specificity} = \frac{TN}{(TN + FP)} \quad (27)$$

Sensitivity, which is also referred to as the true positive rate or recall, holds significant importance as a fundamental performance metric in binary classification tasks, specifically in the field of medical diagnostics, such as tumor detection.

$$\text{Sensitivity} = \frac{TP}{TP + FN} \quad (28)$$

Table 3 presents a complete analysis of specificity and sensitivity, demonstrating the suggested method's excellent capabilities. The NeuroFusionNet outperforms previous works such as the improved residual network (IRN) [24], chronological artificial vultures optimization (CAVO) [27], i-YOLOV5 [26], and whale Harris hawks optimization (WHHO) + deep convolution neural network (DCNN) [28] in terms of specificity and sensitivity. The model's strong specificity reflects its ability to reliably identify real negatives while effectively avoiding false positives. Simultaneously, the model's exceptional sensitivity demonstrates its ability to reliably identify real positives while decreasing false negatives.

In accordance with Table 3, Figure 12 depicts a comparative plot for specificity and sensitivity in the identification of brain tumors. The graphical depiction graphically validates the tabular data, demonstrating NeuroFusionNet's higher performance when compared to alternative approaches. The plot

provides a clear visual proof of the suggested model's high specificity and sensitivity. This comparative graphic clarifies how NeuroFusionNet excels in both minimizing false positives and false negatives, which are critical characteristics in brain tumor diagnosis. The combination of tabular and graphical representations strengthens the case for NeuroFusionNet's supremacy in specific and sensitive brain tumor detection.

Table 3. Specificity and sensitivity values

Techniques used	Specificity (%)	Sensitivity (%)
IRN [24]	76.13	83.5
CAVO [27]	93.8	94.1
i-YOLOV5 [26]	98.78	95.77
WHHO + DCNN [28]	79.1	97.4
Proposed method	99.17	99.383

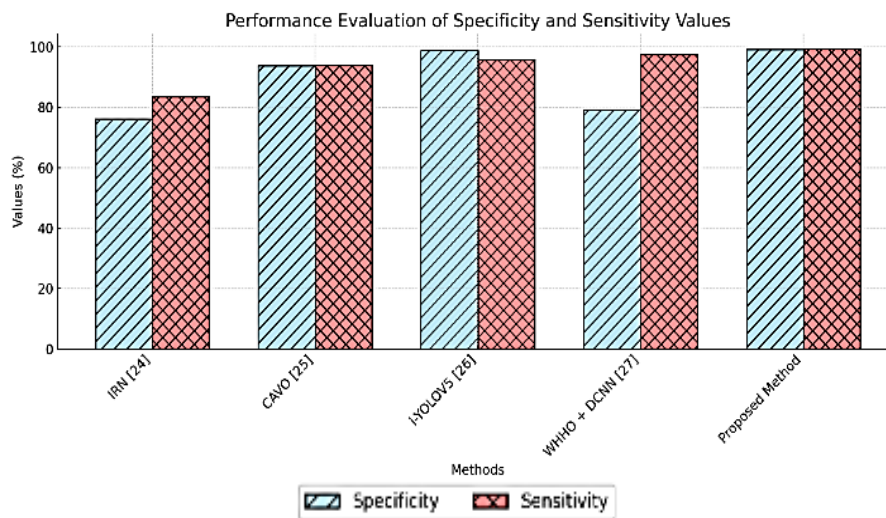


Figure 12. Plot for comparative analysis of specificity and sensitivity

### 4.3. Discussion

This study's findings show that the NeuroFusionNet model is effective at accurately detecting and classifying brain tumors from MRI images. With an overall accuracy of 99.21%, specificity of 99.17%, and sensitivity of 99.383%, the model outperforms several other methodologies. This high level of accuracy demonstrates the model's robustness in distinguishing tumor and non-tumor regions, which is critical for early detection and effective treatment planning. For example, the model's ability to reduce false negatives, as demonstrated by its high sensitivity, ensures that fewer cases of brain tumors go undetected, resulting in better patient outcomes.

In comparison to previous studies, the NeuroFusionNet model significantly improves accuracy and efficiency. For example, the proposed method outperforms Polat and Gungen [17] transfer learning approach (99.02% accuracy) and Hasanah *et al.* [18] machine learning strategy (95.83% accuracy). The combination of advanced image preprocessing techniques and a hybrid deep learning architecture addresses the limitations identified in these studies, such as sensitivity to image quality and the requirement for large annotated datasets. However, the study acknowledges limitations, such as the computational complexity of the NeuroFusionNet model, which may cause problems in terms of processing time and resource availability. Unexpected results, such as a slightly lower specificity than i-YOLOV5 (98.78%), indicate areas for model refinement and optimization.

This study sought to create a robust system for the timely and accurate detection of brain tumors, and the findings highlight the importance of advanced image processing and hybrid deep learning techniques in achieving this goal. The NeuroFusionNet model's superior performance demonstrates its potential as a useful tool in medical diagnostics, laying the groundwork for future research. Unanswered questions remain about the model's applicability to different tumor types and imaging modalities. Future research should focus on improving the model's adaptability and applying it to other medical imaging challenges, ultimately contributing to the advancement of diagnostic technologies and better patient care.

## 5. CONCLUSION

Finally, the importance of early identification in brain tumor instances is obvious, as it allows for faster and more successful therapy interventions. This study aims to contribute to this essential need by developing a reliable brain tumor detection and classification system. The methodology was applied to the BRATS dataset using modern image processing techniques and the NeuroFusionNet hybrid deep learning model, which was specifically built for accurate segmentation. The new model, NeuroFusionNet, outperforms earlier techniques with an accuracy of 99.21% with excellent specificity and sensitivity of 99.17% and 99.383%, respectively. In the future, our research will focus on improving the knowledge and classification of brain tumors by combining the most recent deep learning models. The goal of broadening the scope to identify different types of malignancies is to improve diagnostic precision and give more personalized and effective treatment solutions. Continuous exploration and integration of cutting-edge deep learning techniques will be critical in improving accuracy.




## REFERENCES

- [1] N. Kesav and M. G. Jibukumar, "Efficient and low complex architecture for detection and classification of Brain Tumor using RCNN with Two Channel CNN," *Journal of King Saud University - Computer and Information Sciences*, vol. 34, no. 8, pp. 6229–6242, Sep. 2022, doi: 10.1016/j.jksuci.2021.05.008.
- [2] S. Deepak and P. M. Ameer, "Brain tumor classification using deep CNN features via transfer learning," *Computers in Biology and Medicine*, vol. 111, p. 103345, Aug. 2019, doi: 10.1016/j.compbiomed.2019.103345.
- [3] T. M. Shahriar Sazzad, K. M. Tanzibul Ahmmed, M. U. Hoque, and M. Rahman, "Development of automated brain tumor identification using MRI Images," in *2nd International Conference on Electrical, Computer and Communication Engineering, ECCE 2019*, Feb. 2019, pp. 1–4, doi: 10.1109/ECACE.2019.8679240.
- [4] S. Shanmuga Priya, S. Saran Raj, B. Surendiran, and N. Arulmurugaselvi, "Brain tumour detection in MRI using deep learning," in *Advances in Intelligent Systems and Computing*, vol. 1176, 2021, pp. 395–403, doi: 10.1007/978-981-15-5788-0\_38.
- [5] G. Ankitha, J. Hafsa Tuba, J. Akhilesh, A. Bhanu, and I. G. Naveen, "Brain tumor detection and classification using deep learning approaches," in *2023 4th International Conference for Emerging Technology, INCET 2023*, May 2023, pp. 1–6, doi: 10.1109/INCET57972.2023.10169933.
- [6] N. M. Dipu, S. A. Shohan, and K. M. A. Salam, "Deep learning based brain tumor detection and classification," in *2021 International Conference on Intelligent Technologies, CONIT 2021*, Jun. 2021, pp. 1–6, doi: 10.1109/CONIT51480.2021.9498384.
- [7] M. Arbane, R. Benlamri, Y. Brik, and M. Djerioui, "Transfer learning for automatic brain tumor classification using MRI Images," in *2020 2nd International Workshop on Human-Centric Smart Environments for Health and Well-Being, IHSH 2020*, Feb. 2021, pp. 210–214, doi: 10.1109/IHSH51661.2021.9378739.
- [8] J. Zhang, Z. Jiang, J. Dong, Y. Hou, and B. Liu, "Attention gate ResU-Net for automatic MRI brain tumor segmentation," *IEEE Access*, vol. 8, pp. 58533–58545, 2020, doi: 10.1109/ACCESS.2020.2983075.
- [9] Z. Zhou, M. M. Rahman Siddiquee, N. Tajbakhsh, and J. Liang, "Unet++: A nested u-net architecture for medical image segmentation," in *Lecture Notes in Computer Science (including subseries Lecture Notes in Artificial Intelligence and Lecture Notes in Bioinformatics)*, vol. 11045 LNCS, 2018, pp. 3–11, doi: 10.1007/978-3-030-00889-5\_1.
- [10] M. Alfonso and A.-B. M. Salem, "An automatic classification of brain tumors through MRI using support vector machine," *Egyptian Computer Science Journal*, vol. 40, no. 03, pp. 1110–2586, 2016.
- [11] S. K. Baranwal, K. Jaiswal, K. Vaibhav, A. Kumar, and R. Srikantaswamy, "Performance analysis of brain tumour image classification using CNN and SVM," in *Proceedings of the 2nd International Conference on Inventive Research in Computing Applications, ICIRCA 2020*, Jul. 2020, pp. 537–542, doi: 10.1109/ICIRCA48905.2020.9183023.
- [12] F. Wang *et al.*, "Residual attention network for image classification," *Proceedings - 30th IEEE Conference on Computer Vision and Pattern Recognition, CVPR 2017*, vol. 2017-Janua, pp. 6450–6458, 2017, doi: 10.1109/CVPR.2017.683.
- [13] A. Younis, L. Qiang, C. O. Nyatega, M. J. Adamu, and H. B. Kawuwa, "Brain tumor analysis using deep learning and VGG-16 ensemble learning approaches," *Applied Sciences (Switzerland)*, vol. 12, no. 14, p. 7282, Jul. 2022, doi: 10.3390/app12147282.
- [14] A. Kermi, I. Mahmoudi, and M. T. Khadir, "Deep convolutional neural networks using U-Net for automatic brain tumor segmentation in multimodal MRI volumes," in *Lecture Notes in Computer Science (including subseries Lecture Notes in Artificial Intelligence and Lecture Notes in Bioinformatics)*, vol. 11384 LNCS, 2019, pp. 37–48, doi: 10.1007/978-3-030-11726-9\_4.
- [15] P. Mlynarski, H. Delingette, A. Criminisi, and N. Ayache, "3D convolutional neural networks for tumor segmentation using long-range 2D context," *Computerized Medical Imaging and Graphics*, vol. 73, pp. 60–72, Apr. 2019, doi: 10.1016/j.compmedimag.2019.02.001.
- [16] M. T. Nyo, F. Mebarek-Oudina, S. S. Hlaing, and N. A. Khan, "Otsu's thresholding technique for MRI image brain tumor segmentation," *Multimedia Tools and Applications*, vol. 81, no. 30, pp. 43837–43849, Dec. 2022, doi: 10.1007/s11042-022-13215-1.
- [17] Ö. Polat and C. Güngen, "Classification of brain tumors from MR images using deep transfer learning," *Journal of Supercomputing*, vol. 77, no. 7, pp. 7236–7252, 2021, doi: 10.1007/s11227-020-03572-9.
- [18] U. Hasanah, R. Sigit, and T. Harsono, "Classification of brain tumor on magnetic resonance imaging using support vector machine," *International Electronics Symposium 2021: Wireless Technologies and Intelligent Systems for Better Human Lives, IES 2021 - Proceedings*, pp. 257–262, 2021, doi: 10.1109/IES53407.2021.9594004.
- [19] Z. Huang *et al.*, "Convolutional neural network based on complex networks for brain tumor image classification with a modified activation function," *IEEE Access*, vol. 8, pp. 89281–89290, 2020, doi: 10.1109/ACCESS.2020.2993618.
- [20] H. A. Khalil, S. Darwish, Y. M. Ibrahim, and O. F. Hassan, "3D-MRI brain tumor detection model using modified version of level set segmentation based on dragonfly algorithm," *Symmetry*, vol. 12, no. 8, p. 1256, Jul. 2020, doi: 10.3390/SYM12081256.
- [21] P. Muthu Krishnammal and S. Selvakumar Raja, "Convolutional neural network based image classification and detection of abnormalities in MRI brain images," in *Proceedings of the 2019 IEEE International Conference on Communication and Signal Processing, ICCSP 2019*, Apr. 2019, pp. 548–553, doi: 10.1109/ICCSP.2019.8697915.
- [22] Y. Cheng, G. Qin, R. Zhao, Y. Liang, and M. Sun, "ConvCaps: Multi-input capsule network for brain tumor classification," in *Lecture Notes in Computer Science (including subseries Lecture Notes in Artificial Intelligence and Lecture Notes in*




- Bioinformatics*), vol. 11953 LNCS, 2019, pp. 524–534, doi: 10.1007/978-3-030-36708-4\_43.
- [23] N. Abiwinanda, M. Hanif, S. T. Hesaputra, A. Handayani, and T. R. Mengko, “Brain tumor classification using convolutional neural network,” in *IFMBE Proceedings*, vol. 68, no. 1, 2019, pp. 183–189, doi: 10.1007/978-981-10-9035-6\_33.
- [24] M. Aggarwal, A. K. Tiwari, M. P. Sarathi, and A. Bijalwan, “An early detection and segmentation of brain tumor using deep neural network,” *BMC Medical Informatics and Decision Making*, vol. 23, no. 1, p. 78, Apr. 2023, doi: 10.1186/s12911-023-02174-8.
- [25] B. H. Menze *et al.*, “The multimodal brain tumor image segmentation benchmark (BRATS),” *IEEE Transactions on Medical Imaging*, vol. 34, no. 10, pp. 1993–2024, Oct. 2015, doi: 10.1109/TMI.2014.2377694.
- [26] S. Arunachalam and G. Sethumathavan, “An effective tumor detection in MR brain images based on deep CNN approach: i-YOLOV5,” *Applied Artificial Intelligence*, vol. 36, no. 1, Dec. 2022, doi: 10.1080/08839514.2022.2151180.
- [27] M. Geetha, K. Prasanna Lakshmi, S. R. Arumugam, and N. Sandhya, “Conditional random field-recurrent neural network segmentation with optimized deep learning for brain tumour classification using magnetic resonance imaging,” *Imaging Science Journal*, vol. 71, no. 3, pp. 199–220, Apr. 2023, doi: 10.1080/13682199.2023.2178611.
- [28] D. Rammurthy and P. K. Mahesh, “Whale Harris hawks optimization based deep learning classifier for brain tumor detection using MRI images,” *Journal of King Saud University - Computer and Information Sciences*, vol. 34, no. 6, pp. 3259–3272, Jun. 2022, doi: 10.1016/j.jksuci.2020.08.006.

## BIOGRAPHIES OF AUTHORS



**Arpitha Kotte**    received a Bachelor of Technology (IT) from Mother Teresa College of Engineering, affiliated to JNTU Hyderabad India and Master of Software Engineering in Vaagdevi College of Engineering, affiliated to JNTU Hyderabad, Telangana, India, Pursuing PhD in computer science and engineering from Osmania University, Hyderabad, Telangana India. Sha has published more than 6 peer reviewed international journals and participated in several high-profile conferences. Currently, at present she is working as a solution architect in ready wire Pvt.Ltd product-based company, Hyderabad, Telangana, India. The research is mainly focus on machine learning additionally research includes deep learning, databases and software engineering. She can be contacted at email: kottearpitha87@gmail.com.



**Syed Shabbeer Ahmad**    He received his B.Tech. in computer science and engineering from Sri Venkateswara University in the year 1999, was awarded Ph.D. in computer science and engineering in the area of image processing in 2015 from Shri Venkateswara University. He is currently working as a professor and I/C Head, Department of CSE in MJCET, Hyderabad. He is a ratified professor in computer science and engineering from JNTUH, Hyderabad and Osmania University, Hyderabad. He was also ratified as a Ph.D. research supervisor from Osmania University, Hyderabad in the field of computer science and engineering in the year 2018. He has published 25 research papers in various national/international journals and conferences. He is the recipient of several prestigious awards and grants for his immense contribution in the field of engineering education. He had been the panel member for staff selection committee and BOS member for various colleges and universities. He was a part of the steering committee for the international conferences. He is influential in entering MoUs with different industries/organizations to meet the demand of training and project development on current technologies. Under his guidance innumerable Faculty Development Programs and In-house training programs were conducted to meet the requirements of current industry and research trends. He is a pioneer in initiating innovative activities in the CSE Department at MJCET to train students on latest technologies like web development using PHP, blockchain, artificial intelligence, machine learning and data science. He initiated 24 hrs. Hackathons, summer internships and skill development programs for students in association with Computer Society of India, Microsoft Student Society and IEEE-CS to make them equipped with robust programming and technical skills. With profound knowledge, commendable administrative skill and keen interest in building human network, Prof. Syed Shabbeer Ahmad has built a strong association with the Alumni. It is solely his initiative that some of the alumni even came forward to deliver the sessions on recent trends in the industry. He can be contacted at email: shabbeer.ahmad@mjcollege.ac.in.